Detecting the trapping of small metal nanoparticles in the gap of nanoantennas with optical second harmonic generation

Jérémy Butet,* Andrea Lovera, and Olivier J. F. Martin

Nanophotonics and Metrology Laboratory (NAM), Swiss Federal Institute of Technology Lausanne (EPFL), 1015, Lausanne, Switzerland
**jeremy.butet@epfl.ch*

Abstract: The second harmonic generation from gold nanoparticles trapped into realistic and idealized gold nanoantennas is numerically investigated using a surface integral equations technique. It is observed that the presence of a nanoparticle in the nanoantenna gap dramatically modifies the second harmonic intensity scattered into the far-field. These results clearly demonstrate that second harmonic generation is a promising alternative to the conventional linear optical methods for the detection of trapping events at the nanoscale.

OCIS codes: (160.3900) Metals; (190.0190) Nonlinear optics; (190.2620) Harmonic generation and mixing; (280.4788) Optical sensing and sensors.

References and links

1. J. Prikulis, F. Svedberg, M. Kall, J. Enger, K. Ramser, M. Goksor, and D. Hanstorp, "Optical spectroscopy of single trapped metal nanoparticles in solution," Nano Lett. **4**(1), 115–118 (2004).
2. L. Huang, S. J. Maerkl, and O. J. F. Martin, "Integration of plasmonic trapping in a microfluidic environment," Opt. Express **17**(8), 6018–6024 (2009).
3. W. Zhang, L. Huang, C. Santschi, and O. J. F. Martin, "Trapping and sensing 10 nm metal nanoparticles using plasmonic dipole antennas," Nano Lett. **10**(3), 1006–1011 (2010).
4. M. L. Juan, M. Righini, and R. Quidant, "Plasmon nano-optical tweezers," Nat. Photonics **5**(6), 349–356 (2011).
5. K. Wang, E. Schonbrun, P. Steinvurzel, and K. B. Crozier, "Trapping and rotating nanoparticles using a plamonic nano-tweezer with an integrated heat sink," Nat. Commun. **2**, 469 (2011).
6. A. Lovera and O. J. F. Martin, "Plasmonic trapping with realistic dipole nanoantennas: Analysis of the detection limit," Appl. Phys. Lett. **99**(15), 151104 (2011).
7. M. Kauranen and A. V. Zayats, "Nonlinear plasmonics," Nat. Phys. **6**, 737–748 (2012).
8. B. J. Roxworthy and K. C. Toussaint, Jr., "Femtosecond-pulsed plasmonic nanotweezers," Sci. Rep. **2**, 660 (2012).
9. J. Butet, I. Russier-Antoine, C. Jonin, N. Lascoux, E. Benichou, O. J. F. Martin, and P.-F. Brevet, "Universal scaling of plasmon coupling in metal nanosctructures: Checking the validity for higher plasmonics modes using second harmonic generation," Phys. Rev. B **87**(23), 235437 (2013).
10. J. Butet, I. Russier-Antoine, C. Jonin, N. Lascoux, E. Benichou, and P.-F. Brevet, "Sensing with multipolar second harmonic generation from spherical metallic nanoparticles," Nano Lett. **12**(3), 1697–1701 (2012).
11. G. Bautista, M. J. Huttunen, J. Mäkitalo, J. M. Kontio, J. Simonen, and M. Kauranen, "Second-harmonic generation imaging of metal nano-objects with cylindrical vector beams," Nano Lett. **12**(6), 3207–3212 (2012).
12. V. K. Valev, "Characterization of nanostructured plasmonic surfaces with second harmonic generation," Langmuir **28**(44), 15454–15471 (2012).
13. J. Butet, K. Thyagarajan, and O. J. F. Martin, "Ultrasensitive optical shape characterization of gold nanoantennas using second harmonic generation," Nano Lett. **13**(4), 1787–1792 (2013).
14. H. Shen, N. Nguyen, D. Gachet, V. Maillard, T. Toury, and S. Brasselet, "Nanoscale optical properties of metal nanoparticles probed by second harmonic generation microscopy," Opt. Express **21**(10), 12318–12326 (2013).
15. E. A. Mamonov, T. V. Murzina, I. A. Kolmychek, A. I. Maydykovsky, V. K. Valev, A. V. Silhanek, T. Verbiest, V. V. Moshchalkov, and O. A. Aktsipetrov, "Chirality in nonlinear-optical response of planar G-shaped nanostructures," Opt. Express **20**(8), 8518–8523 (2012).
16. V. K. Valev, B. D. Clercq, X. Zheng, D. Denkova, E. J. Osley, S. Vandendriessche, A. V. Silhanek, V. Volskiy, P. A. Warburton, G. A. E. Vandenbosch, M. Ameloot, V. V. Moshchalkov, and T. Verbiest, "The role of chiral local field enhancements below the resolution limit of second harmonic generation microscopy," Opt. Express **20**(1), 256–264 (2012).

#197706 - $15.00 USD Received 17 Sep 2013; revised 4 Nov 2013; accepted 4 Nov 2013; published 14 Nov 2013

17. J. W. Jarrett, M. Chandra, and K. L. Knappenberger, Jr., "Optimization of nonlinear optical localization using electromagnetic surface fields (NOLES) imaging," J. Chem. Phys. **138**(21), 214202 (2013).
18. M. Scalora, M. A. Vincenti, D. de Ceglia, V. Roppo, M. Centini, N. Akozbek, and M. J. Bloemer, "Second- and third-harmonic generation in metal-based structures," Phys. Rev. A **82**(4), 043828 (2010).
19. C. Ciracì, E. Poutrina, M. Scalora, and D. R. Smith, "Origin of second-harmonic generation enhancement in optical split-ring resonators," Phys. Rev. B **85**(20), 201403 (2012).
20. J. B. Khurgin and G. Sun, "The case for using gap plasmon-polaritons in second-order optical nonlinear processes," Opt. Express **20**(27), 28717–28723 (2012).
21. A. Rose, D. Huang, and D. R. Smith, "Nonlinear interference and unidirectional wave mixing in metamaterials," Phys. Rev. Lett. **110**(6), 063901 (2013).
22. R. Czaplicki, H. Husu, R. Siikanen, J. Mäkitalo, M. Kauranen, J. Laukkanen, J. Lehtolahti, and M. Kuittinen, "Enhancement of second-harmonic generation from metal nanoparticles by passive elements," Phys. Rev. Lett. **110**(9), 093902 (2013).
23. A. M. Kern and O. J. F. Martin, "Surface integral formulation for 3D simulation of plasmonic and high permittivity nanostructures," J. Opt. Soc. Am. A **26**(4), 732–740 (2009).
24. B. Gallinet, A. M. Kern, and O. J. F. Martin, "Accurate and versatile modeling of electromagnetic scattering on periodic nanostructures with a surface integral approach," J. Opt. Soc. Am. A **27**(10), 2261–2271 (2010).
25. J. Mäkitalo, S. Suuriniemi, and M. Kauranen, "Boundary element method for surface nonlinear optics of nanoparticles," Opt. Express **19**(23), 23386–23399 (2011).
26. J. Butet, B. Gallinet, K. Thyagarajan, and O. J. F. Martin, "Second harmonic generation from periodic arrays of arbitrary shape plasmonic nanostructures: A surface integral approach," J. Opt. Soc. Am. B **30**(11), 2970–2979 (2013).
27. A. M. Kern and O. J. F. Martin, "Excitation and reemission of molecules near realistic plasmonic nanostructures," Nano Lett. **11**(2), 482–487 (2011).
28. P. B. Johnson and R. W. Christy, "Optical constants of the noble metals," Phys. Rev. B **6**(12), 4370–4379 (1972).
29. F. X. Wang, F. J. Rodríguez, W. M. Albers, R. Ahorinta, J. E. Sipe, and M. Kauranen, "Surface and bulk contributions to the second-order nonlinear optical response of a gold film," Phys. Rev. B **80**(23), 233402 (2009).
30. G. Bachelier, J. Butet, I. Russier-Antoine, C. Jonin, E. Benichou, and P.-F. Brevet, "Origin of optical second-harmonic generation in spherical gold nanoparticles: Local surface and nonlocal bulk contributions," Phys. Rev. B **82**(23), 235403 (2010).
31. T. V. Raziman and O. J. F. Martin, "Polarisation charges and scattering behaviour of realistically rounded plasmonic nanostructures," Opt. Express **21**(18), 21500–21507 (2013).
32. M. Righini, P. Ghenuche, S. Cherukulappurath, V. Myroshnychenko, F. J. García de Abajo, and R. Quidant, "Nano-optical trapping of Rayleigh particles and Escherichia coli bacteria with resonant optical antennas," Nano Lett. **9**(10), 3387–3391 (2009).
33. M. L. Juan, R. Gordon, Y. J. Pang, F. Eftekhari, and R. Quidant, "Self-induced back-action optical trapping of dielectric nanoparticles," Nat. Phys. **5**(12), 915–919 (2009).
34. J. Zuloaga and P. Nordlander, "On the energy shift between near-field and far-field peak intensities in localized plasmon systems," Nano Lett. **11**(3), 1280–1283 (2011).
35. B. Metzger, M. Hentschel, M. Lippitz, and H. Giessen, "Third-harmonic spectroscopy and modeling of the nonlinear response of plasmonic nanoantennas," Opt. Lett. **37**(22), 4741–4743 (2012).
36. E. Prodan, C. Radloff, N. J. Halas, and P. Nordlander, "A hybridization model for the plasmon response of complex nanostructures," Science **302**(5644), 419–422 (2003).
37. L. Huang and O. J. F. Martin, "Reversal of the optical force in a plasmonic trap," Opt. Lett. **33**(24), 3001–3003 (2008).
38. J. Berthelot, G. Bachelier, M. Song, P. Rai, G. Colas des Francs, A. Dereux, and A. Bouhelier, "Silencing and enhancement of second-harmonic generation in optical gap antennas," Opt. Express **20**(10), 10498–10508 (2012).
39. B. K. Canfield, H. Husu, J. Laukkanen, B. Bai, M. Kuittinen, J. Turunen, and M. Kauranen, "Local field asymmetry drives second-harmonic generation in non-centrosymmetric nanodimers," Nano Lett. **7**(5), 1251–1255 (2007).
40. N. Yang, W. E. Angerer, and A. G. Yodh, "Angle-resolved second-harmonic light scattering from colloidal particles," Phys. Rev. Lett. **87**(10), 103902 (2001).
41. B. Schürer, S. Wunderlich, C. Sauerbeck, U. Peschel, and W. Peukert, "Probing colloidal interfaces by angle-resolved second harmonic light," Phys. Rev. B **82**(24), 241404 (2010).
42. G. Gonella, W. Gan, B. Xu, and H.-L. Dai, "The effect of composition, morphology, and susceptibility on nonlinear light scattering from metallic and dielectric nanoparticles," J. Phys. Chem. Lett. **3**(19), 2877–2881 (2012).
43. J. I. Dadap, J. Shan, and T. F. Heinz, "Theory of optical second-harmonic generation from a sphere of centrosymmetric materials: small-particle limit," J. Opt. Soc. Am. B **21**(7), 1328–1347 (2004).
44. J. Butet, J. Duboisset, G. Bachelier, I. Russier-Antoine, E. Benichou, C. Jonin, and P.-F. Brevet, "Optical second harmonic generation of single metallic nanoparticles embedded in a homogeneous medium," Nano Lett. **10**(5), 1717–1721 (2010).

#197706 - $15.00 USD Received 17 Sep 2013; revised 4 Nov 2013; accepted 4 Nov 2013; published 14 Nov 2013

45. H. Fischer and O. J. F. Martin, "Engineering the optical response of plasmonic nanoantennas," Opt. Express **16**(12), 9144–9154 (2008).
46. K. C. Neuman and S. M. Block, "Optical trapping," Rev. Sci. Instrum. **75**(9), 2787–2809 (2004).
47. F. Gittes and C. F. Schmidt, "Interference model for back-focal-plane displacement detection in optical tweezers," Opt. Lett. **23**(1), 7–9 (1998).

1. Introduction

The optical trapping of nanosized objects provides interesting opportunities for the development of new applications in nanophotonics [1]. While the far-field trapping of objects smaller than the incident wavelength is quite difficult to achieve, it was recently shown that plasmon nano-optical tweezers allow for the trapping of nano-objects [2–5]. Plasmon nano-optical tweezers take advantage of the strong localization of the electric field induced by localized surface plasmon resonances (LSPR) to tailor the trapping potential making the trapping time longer [2–5]. Since trapping events cannot be directly observed for extremely small nanosized objects, it is necessary to track them by indirect measurements. As an example, one can observe a trapping event by monitoring the spectral position shift of the LSPR sustained by the optical trap. The shift amplitude depends on the optical trap properties as well as the nature of the trapped object [6]. Depending on the experimental conditions, the shift amplitude can be small and the observation of trapping events challenging. As a consequence, it is necessary to develop new detection techniques to make such an observation easier. One possibility is to use parametric nonlinear optical processes [7, 8]. Indeed, it was recently shown that second harmonic generation (SHG) opens up new possibilities for determining the properties of SPR [9] and for practical applications such as nonlinear plasmonic sensing [10], shape characterization [11–14], and imaging [15–17]. Furthermore, SHG from metal metamaterials was also intensively studied [18–22].

In the present article, the detection of trapping events with dipole nanoantennas using second harmonic (SH) far-field is investigated numerically. Using surface integral equation techniques, both the linear and the SH responses of coupled gold nanoantenna and nanoparticle systems are computed. Both idealized and realistic nanoantennas are considered, emphasizing that SHG is an alternative tool to the conventional LSPR shift measurements for monitoring trapping events in experimentally realizable plasmonic nano-optical tweezers. Finally, the detection limit of this approach in terms of particle size is discussed.

2. Results and discussion

The numerical calculations presented in this article have been performed with surface integral equation methods. These methods have already been described elsewhere [23–26] and were used for the analysis of both the linear and SH responses of plasmonic nanostructures [11, 13, 25, 27]. All the considered nanoantennas are in a water environment (n = 1.33) and the dielectric constant of gold is taken from experimental data [28]. The nanoantennas are driven by an incident plane wave propagating along the *z*-axis and linearly polarized along the *x*-axis, see Fig. 1. Only a surface contribution to the SHG is considered in this work [29, 30], and the surface of the plasmonic nanostructures is discretized with an adaptive triangular mesh with typical side of 5 nm but smaller triangles are used to describe the rounded nanocorners and the spherical nanoparticles [31]. The approximate side length of the triangle mesh is respectively 1.25 nm, 0.7 nm, and 0.4 nm for the description of the 20 nm, 10 nm, and 5 nm spherical nanoparticles. Note that the present work focuses on the detection of metal nanoparticles but the detection of dielectric spheres is also of practical interest and will be addressed in the future [32, 33].

2.1 Idealized nanoantenna

Let us first consider an ideal nanoantenna composed of two 100 nm long 40 x 40 nm^2 section rectangular arms with 5 nm rounded corners separated by a 25 nm nanogap. The scattering spectrum exhibits a resonance peak at the wavelength λ = 840 nm (data not shown). Note that

#197706 - $15.00 USD Received 17 Sep 2013; revised 4 Nov 2013; accepted 4 Nov 2013; published 14 Nov 2013

the maximum of the extinction spectrum does not necessary correspond to the maximal near-field enhancement in general and the exact spectral position of the maximal SHG efficiency cannot be directly determined from the linear scattering spectrum [34]. In order to avoid such an indeterminacy in the following analysis, the incident wavelength is first chosen shorter than the LSPR (incident wavelength λ = 730 nm) [35]. Furthermore, the observation of SHG from plasmonic nanostructures requires femtosecond optical pulses, the bandwidth of which can be larger than the plasmon shift, making the determination of LSPR maximum complicated. The influence of a 20 nm gold nanoparticle located in the nanogap on the fundamental (linear) near-field distributions is discussed first.

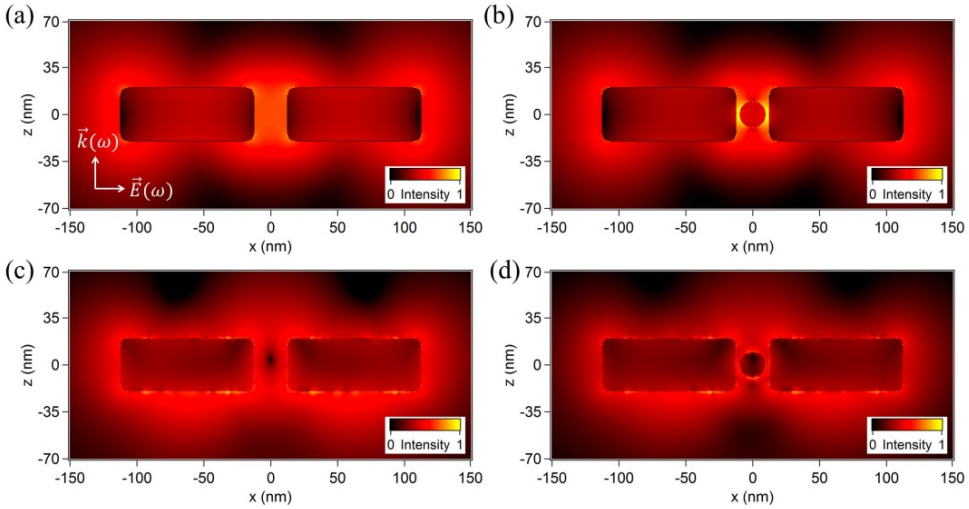

Fig. 1. Normalized near-field intensity distributions evaluated at the (a)-(b) fundamental and (c)-(d) SH wavelength (all shown in a logarithmic scale) close to an idealized antenna without (left-hand side panels) and with a 20 nm gold nanoparticle in the nanogap (right-hand side panels). The nanogap is 25 nm long. The fundamental and SH wavelengths correspond to λ = 730 nm and λ = 365 nm, respectively. Note that the color scales are identical for the panels (a) and (b) and for the panels (c) and (d).

Figure 1 shows the near-field intensity distribution at the fundamental wavelength in the case of both (a) the bare nanoantenna and (b) the antenna with a 20 nm gold nanoparticle trapped in the center of the nanogap (nanoparticle position: $x = 0$ nm, $y = 0$ nm, and $z = 0$ nm). A direct comparison indicates that the near-field intensity, evaluated at the end of the nanoantenna arm ($x = -113$ nm, $y = 0$ nm, and $z = 0$ nm) is decreased by 34% when a nanoparticle is trapped in the nanogap. Indeed, the inclusion of a 20 nm gold nanoparticle in the nanogap redshifts the LSPR by approximately 5 nm. The LSPR shift is induced by the hybridization between the modes of the trapped plasmonic nanoparticle and the trapping nanoantenna [6, 36]. The near-field intensity decrease indicates that the presence of the gold nanoparticle shifts the SPR away from the incident wavelength (λ = 730 nm) [37]. Although the detection limit of this shift in the linear regime has been widely studied in the past, this is not the case for nonlinear optical processes. For a detailed discussion of the linear case, the reader is referred to our previous publication [6]. The corresponding SH near-field distributions have been computed and the results are shown in Figs. 1(c) and 1(d). Contrary to the linear case, the SH near-field intensity is not as much enhanced when a gold nanoparticle is present in the nanogap. Note further that the SH intensity at the extremities of the antenna is even lower when a particle is trapped in the gap, compare Figs. 1(c) and 1(d). It is worth to note that the SH intensity minimum observed in the empty nanogap is due to destructive interferences between the nonlinear sources [38]. Despite a strong enhancement of the fundamental electric field in the nanogap, this non-radiative behavior is also expected when a

#197706 - $15.00 USD Received 17 Sep 2013; revised 4 Nov 2013; accepted 4 Nov 2013; published 14 Nov 2013

nanoparticle is located at the nanogap center since the centrosymmetry is conserved [39]. The SH far-field properties will now be discussed in detail.

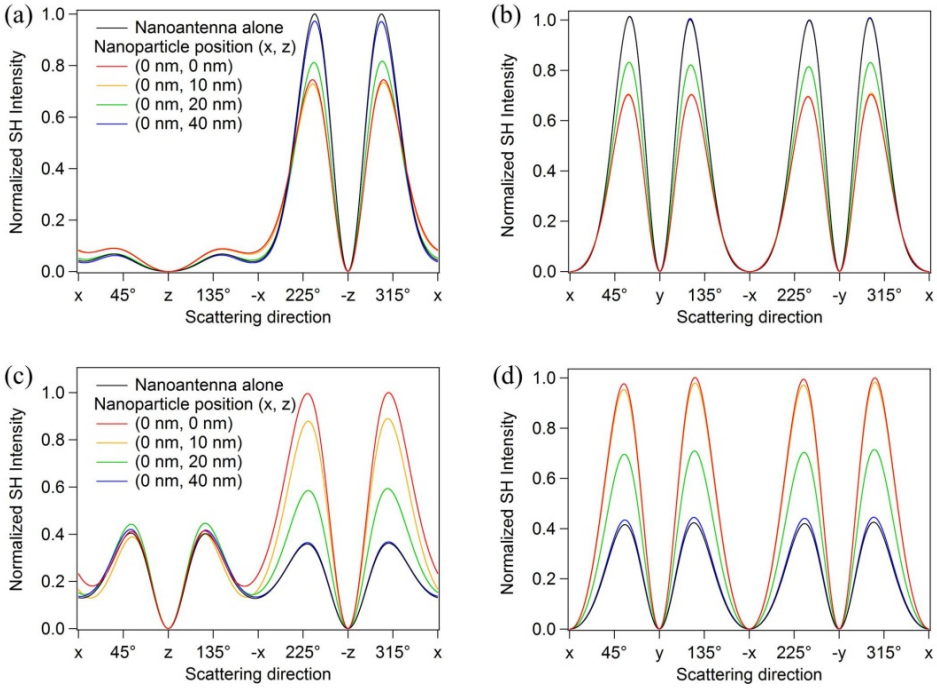

Fig. 2. (a) Normalized SH intensity scattered in the horizontal plane calculated in the case of the bare idealized nanoantenna and with a 20 nm gold nanoparticle at different positions; (b) Normalized SH intensity scattered in the vertical plane calculated considering the SH scattered wave polarized into the (O, *x*, *y*) plane in the case of the bare idealized nanoantenna and with a 20 nm gold nanoparticle at different positions. The nanogap is 25 nm long and the incident wavelength is λ = 730 nm. The panels (c) and (d) correspond to identical computation parameters as the panels (a) and (b), respectively, but for an incident wavelength λ = 860 nm.

In order to determine the influence of a trapped nanoparticle on the SH far-field emission and to quantify the prospect of remote detection of trapping events using SHG, we show in Fig. 2 the normalized SH intensity scattered in the horizontal (O, *x*, *z*) plane and the vertical (O, *x*, *y*) plane, computed in the far-field (evaluated 50 μm away from the antenna) as a function of the scattering direction. This corresponds to angle-resolved SH light scattering measurements [40–42]. In addition to positioning the trapped particle in the center of the gap, we also now investigate the SH intensity for other positions keeping the nanoparticle close to the nanogap, see Fig. 2. Displacements of the trapped nanoparticle along the z- and y-directions are expected to provide the same kind of response since this antenna is symmetric in these two directions. On the contrary, any displacements along the x-direction are not expected to induce an important LSPR shift since the amplitude of the displacements along this direction is limited by the nanogap dimension and the near-field intensity in the nanogap is almost constant when the coordinate *x* varies. For all the investigated configurations, a four lobes pattern is observed in the vertical plane. This emission pattern is characteristic of a quadrupolar SH emission [43, 44]. Such an observation is not surprising since SHG from centrosymmetric metal nanostructures is forbidden in the electric dipole approximation [43, 44]. As observed for the SH near-field intensity, the SH intensity scattered into the far-field decreases due to the presence of the gold nanoparticle and its influence on the LSPR. When the nanoparticle is situated at the nanogap center, the intensity of the two lobes observed between –x and x in the horizontal plane drops by 25%, see Fig. 2(a). On the other hand, the

#197706 - $15.00 USD Received 17 Sep 2013; revised 4 Nov 2013; accepted 4 Nov 2013; published 14 Nov 2013

intensity of the four lobes observed in the vertical plane decreases by 30%, see Fig. 2(b). The impact on the trapped nanoparticle on the nonlinear response decrease when the nanoparticle is not situated at the nanogap center. Indeed, the coupling between the nanoparticle and the nanoantenna depends on their relative position and the SH intensity is minimum when the nanoparticle is at the gap center i. e. when the plasmon coupling is the strongest [6, 36].

Let us address the spectral flexibility of SHG as a tool for detection of trapping events at the nanoscale. Further computations of the SH far-field distribution have been performed considering an incident plane wave at a longer wavelength than the bare nanoantenna LSPR (incident wavelength λ = 860 nm). When the nanoparticle is situated at the nanogap center, the intensity of two lobes observed between –x and x in the horizontal plane is multiplied by 2.8, while the intensity of the 4 lobes observed in the vertical plane is multiplied by 2.4. In summary, the trapping of a nanoparticle leads to an increase or a decrease of the scattered SH intensity depending if the incident wavelength is shorter or longer than the initial LSPR supported by the nanoantenna. This result underlines the flexibility of SHG as a new method for the detection of trapping events since the incident wavelength does not need to be accurately tuned at the LSPR maximum. Nevertheless, the nanofabrication of regular plamonic antennas is difficult to achieve and the presence of morphology defects is known to modify their near-field optical response [27]. For this reason, in the next section we consider more realistic nanoantennas shapes [6].

2.2 Realistic nanoantenna

Let us now investigate SH measurements of the trapping in a more realistic nanoantenna. Indeed, it was recently shown that the morphology of a plasmonic nanoantenna strongly influences the SH signal, even when the linear response is not affected [13]. The mesh used for the realistic nanoantenna here has been adapted from a scanning electron microscope image [27]. The two arms are 100 nm long and the gap distance is 25 nm. The resonance wavelength is λ = 710 nm. Note that results discussed in this article are general and independent of the LSPR spectral position. Figure 3 shows the fundamental near-field intensity distributions for the bare nanoantenna and with a 20 nm gold nanoparticle trapped in the nanogap (nanoparticle position: x = 0 nm, y = 0 nm, and z = 0 nm). As observed when the

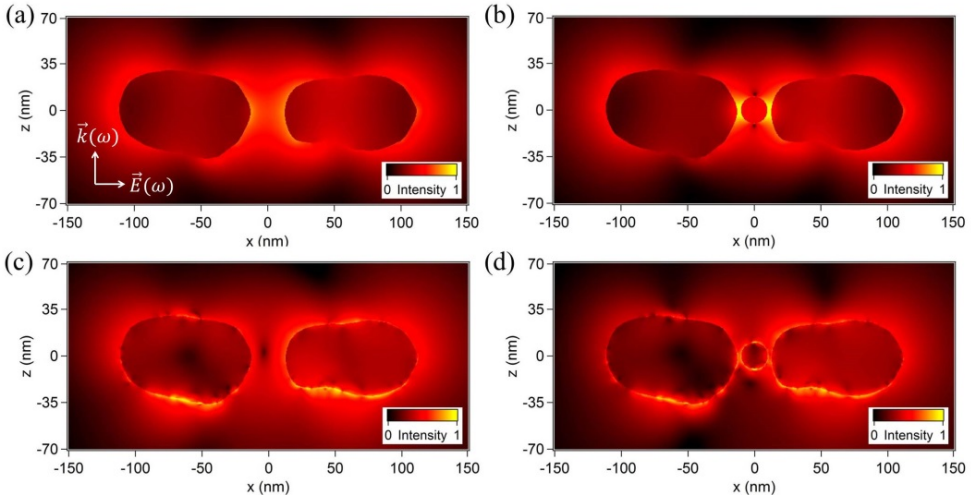

Fig. 3. Normalized near-field intensity distributions evaluated at the (a)-(b) fundamental and (c)-(d) SH wavelength close to a realistic antenna without (left hand side panels) and with a 20 nm gold nanoparticle in the nanogap (right hand side panels). The nanogap is 25 nm long. The fundamental and SH wavelengths are λ = 710 nm and λ = 355 nm, respectively. Note that the color scales are identical for the panels (a) and (b) and for the panels (c) and (d).

#197706 - $15.00 USD Received 17 Sep 2013; revised 4 Nov 2013; accepted 4 Nov 2013; published 14 Nov 2013

idealized nanoantenna is driven by a plane wave with a wavelength matching its LSPR, the trapping of a gold nanoparticle induces an enhancement of the fundamental electric field in the nanogap as well as a decrease of the fundamental electric field at the nanoantenna arm ends resulting from the LSPR shift. The SH near-field intensity distributions computed for the realistic nanoantenna are shown in Figs. 3(c) and 3(d).

As in the case of the idealized nanoantenna, the SH intensity scattered into the far-field is evaluated in both the vertical and horizontal planes as a function of the scattering direction, see Figs. 4(a) and (b). The emission patterns are not as symmetric as the ones observed for the idealized nanoantenna but the impact of the trapped gold nanoparticle on the SH response is still clearly visible. Contrary to the previous observation made for the idealized nanoantenna, the SH intensity increases or decreases depending on the scattering direction. This behavior is explained by the non-centrosymmetric shape of the realistic nanoantenna gap. The interferences between the nonlinear sources standing close to the nanogap are not fully destructive and an augmentation of the fundamental near-field intensity tends to increase the SH signal scattered in the far-field [39]. On the contrary, the shift of the LSPR induces a decrease of the fundamental near-field intensity and tends to decrease the SH signal. Due to the interplay between these two effects, the overall SH conversion yield is almost not modified by the trapped nanoparticle when the incident wavelength matches the LSPR of the bare realistic nanoantenna. In order to further investigate this interplay between enhancement and lowering of the SH signal, further simulations have been performed considering an incident wavelength longer than the bare nanoantenna LSPR. Figures 4(c) and 4(d) show the SH intensity far-field distribution considering an incident wavelength λ = 750 nm. In this case, both the LSPR shift and enhancement of the fundamental electric field in the nanogap tend to increase the SH conversion efficiency. As a result, the SH intensity is increased in almost all the scattering directions and the trapping of a gold nanoparticle can be detected in various experimental configurations. Furthermore, the symmetry of the experimental system is broken when realistic nanoantennas are considered and displacement of the trapped nanoparticle along y- and x-directions is also detectable.

Finally, the detection limit of trapping events in the nonlinear regime is considered. Computations have been performed considering gold nanoparticles with smaller diameters (5 nm and 10 nm. The presence of smaller gold nanoparticles in the nanogap also results in change of the SH intensity far-field distribution. The maximal variation of the lobe intensity is 8% for the 10 nm gold nanoparticle but less than 2% for the 5 nm one, demonstrating that small nanoparticles are barely observed. Nevertheless, the electric field enhancement in the nanogap increases with decreasing nanogap dimensions, allowing to detect smaller nanoparticles [6]. Indeed, it was shown that the LSPR shift is proportional to the near-field intensity felt by the trapped nanoparticle [6]. Finally, we consider a realistic antenna with a shorter gap of 15 nm, keeping the arm length constant. The resonant wavelength is then shifted to 730 nm. Indeed, the plasmonic coupling increases with decreasing gap distance, resulting in a longer resonant wavelength [45]. Computations of the SH far-field distribution have been performed considering an incident plane wave with a wavelength λ = 730 nm, see Fig. 5(b). In this case, the maximal lobe intensity variation is 23% for the 10 nm gold nanoparticle and almost 5% for the 5 nm one demonstrating that the detection limit can be increased if the nanoantenna dimensions are optimized. Further simulations have been performed considering a gold nanoparticle close to the nanoantenna but not in the nanogap. The SH response has been computed for a 20 nm nanoparticle located laterally on the gap (x = 40 nm) of the realistic nanoatenna with a 25 nm gap and comparison with the bare nanoantenna shows no modification of the nonlinear response as it was previously reported in the linear regime [6]. As a consequence, the detection of trapping events in this configuration is not expected to be more sensitive using SHG than considering the linear response.

#197706 - $15.00 USD Received 17 Sep 2013; revised 4 Nov 2013; accepted 4 Nov 2013; published 14 Nov 2013

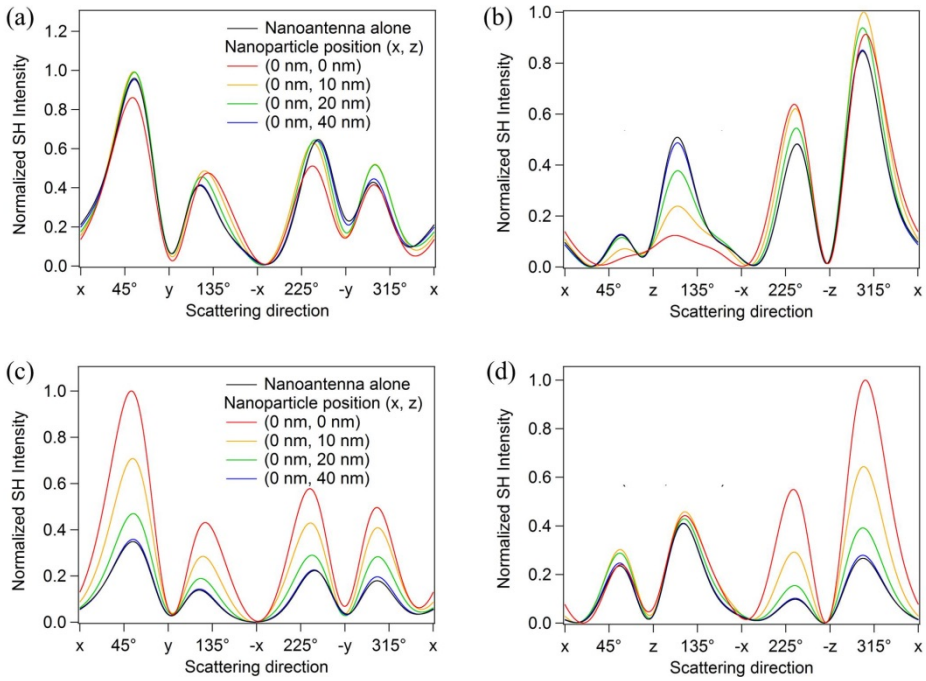

Fig. 4. (a) Normalized SH intensity scattered in the vertical plane calculated considering the SH scattered wave polarized into the (O, *x*, *y*) plane in the case of the bare realistic nanoantenna and with a 20 nm gold nanoparticle at different positions. (b) Normalized SH intensity scattered in the horizontal plane calculated in the case of the bare realistic nanoantenna and with a 20 nm gold nanoparticle situated at different positions. The incident wavelength is λ = 710 nm. The panels (c) and (d) correspond to identical computation parameters as the panels (a) and (b), respectively, but for an incident wavelength λ = 750 nm.

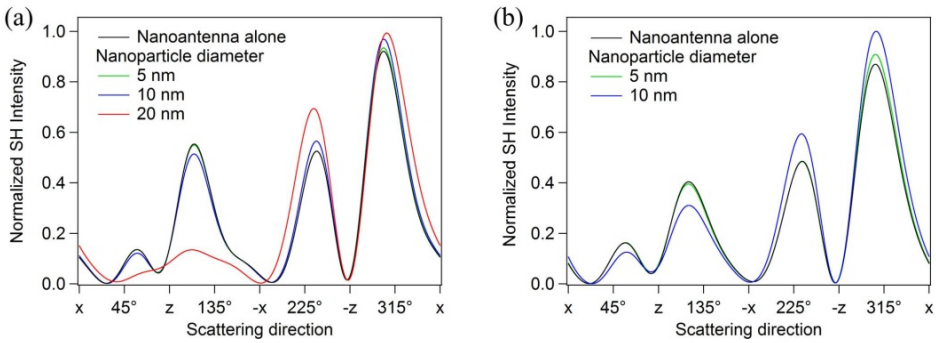

Fig. 5. Normalized SH intensity scattered in the horizontal plane calculated in the case of the bare realistic nanoantenna and with a gold nanoparticle with various diameters situated at the nanogap center. (a) The nanogap is 25 nm long and the incident wavelength is λ = 710 nm. (b) The nanogap is 15 nm long and the incident wavelength is λ = 730 nm.

3. Conclusions

In summary, the detection of metal nanoparticles in the nanogap of dipolar nanoantennas using SHG has been numerically investigated using a surface integral equation method. Considering idealized nanoantennas, it was shown that the trapping of a metal nanoparticle in the nanogap results in an increase of the SH intensity if the SPR is shifted closer to the incident wavelength or in a decrease of the SH intensity if the SPR is shifted away from the

#197706 - $15.00 USD Received 17 Sep 2013; revised 4 Nov 2013; accepted 4 Nov 2013; published 14 Nov 2013

incident wavelength. As a consequence, the incident wavelength does not need to be tuned at the SPR maximum to detect a trapping event, thus emphasizing the flexibility of SHG for sensing purposes. The case of realistic nanoantennas was also addressed demonstrating that SHG allows to observe trapping events even in more realistic experimental conditions. The variation of the SH intensity is observed for gold nanoparticles as small as 5 nm if the dimensions of the nanoantenna are optimized demonstrating that SHG is a promising alternative to the conventional linear optical methods for the detection of trapping events at the nanoscale. Furthermore, the numerical results presented in this article demonstrate that SHG makes possible the characterization of the optical trap and the determination of its properties, like for example the trap stiffness and the trapping time [46]. Indeed, a 10 nm displacement of a nanoparticle trapped in the gap of a realistic nanoantenna can induce a variation of the SH intensity as high as 50%, providing real-time information of the nanoparticle location inside the trap. For example, it is then possible to replace linear scattering by SHG in the quadrant detection scheme for the determination of trap stiffness [47].

Acknowledgments

It is a pleasure to acknowledge stimulating discussion with Krishnan Thyagarajan, and T. V. Raziman and Shourya Dutta-Gupta for helpful discussions about the impact of rounded corners on the optical properties of nanoantennas. This work was supported by the Swiss National Science Foundation (grant 200021-125326) and by European Community's Seventh Framework Program (FP7-ICT-2009-4, Grant agreement 248835).

#197706 - $15.00 USD Received 17 Sep 2013; revised 4 Nov 2013; accepted 4 Nov 2013; published 14 Nov 2013